Interparticle Potential and the Phase Behavior of Temperature-Sensitive Microgel Dispersions

Jianzhong Wu*

Department of Chemical and Environmental Engineering, University of California, Riverside, California 92521

Gang Huang and Zhibing Hu

Departments of Physics and Chemistry, University of North Texas, P.O. Box 311427, Denton, Texas 76203

Received September 9, 2002; Revised Manuscript Received November 4, 2002

ABSTRACT: Molecular−thermodynamic models assisted with experimental measurements are applied to correlate and predict the volume transition and structural ordering of poly(*N*-isopropylacrylamide) (PNIPAM) microgel particles dispersed in pure water. The effective pair potential between PNIPAM particles is represented by a Sutherland-like potential where the size and energy parameters are correlated with particle radius and the solution osmotic second virial coefficients attained from static and dynamic light scattering experiments. Using a first-order perturbation theory for the fluid phase and an extended cell model for the crystalline solid, the calculated phase diagram indicates that an aqueous dispersion of PNIPAM particles may freeze at both high and low temperatures. At low temperature, the freezing occurs at large particle volume fraction, similar to that in a hard-sphere system, while at high temperature, the freezing is driven by strong van der Waals attraction due to the increase in the Hamaker constant of the microgel particles when they collapse. The phase diagram of PNIPAM dispersions predicted from the molecular−thermodynamic models agrees favorably with experimental observations.

1. Introduction

Over the past decade colloidal dispersions have been a subject of intensive investigations.[1−3] On one hand, colloidal dispersions provide model systems for studying the long-standing fundamental questions on the nature of liquids, solids, and glasses; on the other hand, self-assembly of colloidal particles has been extensively used as templates for the fabrication of nanostructured materials.[4,5] Amid numerous conventional colloids, aqueous dispersions of poly(*N*-isopropylacrylamide) (PNIPAM) microgel particles, first synthesized by Pelton and Chibante in 1986,[6] are of special interest for studying the phase transitions and for the fabrication of colloid-based advanced materials.[7,8] Nearly monodispersed PNIPAM particles now can be routinely prepared in a wide range of colloidal sizes (50 nm up to 1 μm) and with a variety of physiochemical characterizations.[7,9] By tuning the preparation conditions and the composition of the aqueous solution, the interaction potential between microgel particles can vary from star-polymer-like to hard-sphere-like potential for short-range repulsion, from electrostatically neutral to highly ionizable for long-range electrostatic interactions, and from essentially no attraction to strong attraction for the van der Waals forces.[8,10] Furthermore, steric repulsion can be introduced by grafting polymers on the surface of PNIPAM particles.[11] The versatility in the interaction potential makes PNIPAM microgel particles attractive for studying a broad variety of interesting phenomena in colloidal systems.[12−16]

Like their macroscopic counterparts, PNIPAM particles may undergo a drastic volume change in responding to small variances in the aqueous environment, such as temperature, ionic strength, or pH.[7] The volume transition of the PNIPAM gel is closely related to the coil−globule transition of the PNIPAM chains and has been explained using the Flory−Huggins theory.[17] Because of the unique physiochemical properties, microgel particles are promising for a broad variety of applications. Assembly of microgel particles has been proposed to be used as drug carriers,[18] artificial biomaterials,[19] photonic crystals,[12,20−22] and separation media.[23,24] While microgel particles retain the unique physical properties of bulk hydrogels, swelling/deswelling kinetics of microgel particles is much faster in comparison to macrogels. For many practical applications, rapid response to environmental stimuli is of crucial importance.

Although the practical values of PNIPAM particles have been long recognized, most previous studies on the physiochemical properties of PNIPAM dispersions have been focused on the particle preparations, swelling, rheology, and light (neutron) scattering measurements.[7,8,25−27] Little work has been reported on the relationship between the temperature-dependent interparticle potential and the phase behavior of PNIPAM dispersions. Unlike that in a conventional colloidal system, the interparticle potential in aqueous dispersion of PNIPAM microgel particle is sensitive to the temperature changes. Consequently, the phase diagram of PNIPAM dispersions may be noticeably different from those for ordinary colloids where, in most cases, the interparticle potential is essentially invariant with temperature.

In this work, we report the phase behavior of neutral PNIPAM particles dispersed in pure water. Differing from most previous studies on the phase diagrams of colloidal systems, we start with investigations on the interparticle potential using both dynamic and static light-scattering measurements. A modified Flory−Re-

* Corresponding author: e-mail jwu@engr.ucr.edu.

10.1021/ma025656m CCC: $25.00
Published on Web 12/14/2002

hner theory, which takes into consideration the microgel heterogeneity, is used to correlate the diameter of PNIPAM particle as a function of temperature.[28] The phase diagram is then calculated using a first-order perturbation theory for the fluid phase and an extended cell model for the crystalline solid. Finally, the phase behavior of the microgel dispersions predicted from thermodynamic perturbation is compared with observations from spectroscopic measurements.

2. Experiment

2.1. Materials. *N*-Isopropylacrylamide was obtained from Polysciences Inc. and used as received. The cross-linker *N,N′*-methylenebis(acrylamide) (MBAAm) was purchased from Bio Rad Co. The sodium dodecyl sulfate (SDS) and potassium persulfate (KPS) were both bought from Aldrich Chemical Co and used as received. Distilled and deionized water (resistance of 18 MΩ·cm) was used throughout. A 0.5 μm Millipore (Millex LCR25) filter was used to purify the dilute sample solutions.

2.2. Sample Preparation. Narrowly distributed PNIPAM microgel particles were synthesized following the pioneering work by Pelton.[7] 1.54 g of NIPAM monomer, 0.0262 g of MBAAm, 0.0439 g of sodium dodecyl sulfate (SDS), and 90 mL of deionized water were mixed in the flask. The solution was stirred at 300 rpm for 30 min under a nitrogen environment. 0.0624 g of KPS dissolved in 10 mL of deionized water was added to start the reaction. The reaction was carried out at 70 °C for 4 h. The reaction was kept at 68−70 °C under nitrogen for 4 h to ensure that all the monomer was reacted. After cooling to room temperature, the dispersion was exhaustively dialyzed in a dialysis tube for 7 days. The deionized water out of the tube was changed three times every day. The PNIPAM particle dispersions were condensed using an ultracentrifuge with speed of 40 000 rpm for 2 h.

2.3. Laser Light Scattering (LLS). A commercial laser light scattering (LLS) spectrometer (ALV/DLS/SLS-5000) equipped with an ALV-5000 digital time correlator was used with a helium−neon laser (Uniphase 1145P, output power of 22 mW and wavelength of 632.8 nm) as the light source. The incident light was vertically polarized with respect to the scattering plane, and the light intensity was regulated with a beam attenuator (Newport M-925B). The scattered light was conducted through a thin (∼100 μm in diameter) optic fiber leading to an active quenched avalanche photodiode (APD). The coherent factor β in dynamic laser light scattering was 0.98 for our instrument. The avalanche photodiode had a sensitivity 2 orders of magnitude higher than that of a normal photon multiplier (PM) tube, while its dark count increased no more than 10 times so that a 22 mW laser could have a measured count rate (scattered intensity) similar to a 400 mW laser for a normal photomultiplier tube.

In static light scattering (SLS), we measure the angular dependence of the excess Rayleigh ratio $R_{vv}(q)$ of dilute PNIPAM dispersions. $R_{vv}(q)$ is related to the weight-average molar mass M_w, the second virial coefficient B_2, and the *z*-average root-mean-square radius of gyration $\langle R_g^2\rangle_z^{1/2}$ (or simply $\langle R_g\rangle$) by[29]

$$\frac{KC}{R_{vv}(q)} \cong \frac{1}{M_w}\left(1 + \frac{1}{3}\langle R_g^2\rangle q^2\right) + 2B_2C \qquad (1)$$

where $K = 4\pi^2 n^2 (dn/dC)^2/(N_A\lambda_0^4)$ and $q = (4\pi n/\lambda_0)\sin(\theta/2)$ with N_A, n, C, λ_0, and θ being Avegadro's constant, the solvent refractive index, the solid concentration (g/cm^3 or g/g), the light wavelength in the vacuum, and the scattering angle, respectively. In SLS, the samples were scanned from angle 30° to 120° with a 5° interval. The dn/dC value of PNIPAM in water was taken as 0.167 cm^3/g from reference 30 without wavelength correction. (As a result, the molar masses obtained in our measurements are the apparent values.)

In dynamic light scattering (DLS), the intensity−intensity correlation function $G^{(2)}(\tau,\theta)$ is measured, which is related to the normalized first-order electric field time correlation function $|g^{(1)}(\tau,\theta)|$ by the Siegert relation[30,31]

$$G^{(2)}(\tau,\theta) = \langle I(0,\theta)\, I(\tau,\theta)\rangle = A[1+\beta|g^{(1)}(\tau,\theta)|^2] \qquad (2)$$

where τ is the delay time, A is measured baseline, and β is the coherent factor of the detection. For a polydisperse sample, $|g^{(1)}(\tau,\theta)|$ is related to the decay rate (Γ) distribution $G(\Gamma)$

$$|g^{(1)}(\tau,\theta)| = \int_0^\infty G(\Gamma)e^{-\Gamma\tau}\,d\Gamma \qquad (3)$$

In this study both the CONTIN program developed by Provencher[32] and the cumulant analysis are used to calculate $G(\Gamma)$, and they lead to consistent results. In general, the relaxation rate Γ is a function of both the colloidal concentration C and the scattering vector q. For a diffusive relaxation at infinite dilution of colloids, these effects can be expressed as

$$\Gamma/q^2 = D \qquad (4)$$

where D is the translational diffusion coefficient at $C \to 0$ and $q \to 0$, which is related to the hydrodynamic radius (R_h) by the Stokes−Einstein equation, $R_h = kT/6\pi\eta D$, where k, η, and T are the Boltzmann constant, the solvent viscosity, and the absolute temperature, respectively. The DLS measurements were carried out at the scattering angle $\theta = 60°$.

2.4. Phase Diagram Measurement. A quantitative phase diagram of PNIPAM dispersions can be constructed by measuring the UV−vis absorbance spectra on a diode array spectrometer (Hewlett-Parkard, model 8543) with the wavelength ranging from 190 to 1100 nm. The turbidity of the samples was obtained from the ratio of the transmitted light intensity (I_t) to the incident intensity (I_0) as $\alpha = -(1/L)\ln(I_t/I_0)$, where L was the sample thickness (1 cm). In the crystalline phase, the UV−vis spectrum exhibits a sharp attenuation peak due to the Bragg diffraction. Above the crystalline melting temperature, the peak disappears. On the other hand, as the temperature rises to the phase separation temperature, the turbidity increases sharply in the entire range of visible light wavelengths.

3. Theory

3.1. Volume Transition of PNIPAM Particles. The classical theory of gel swelling, proposed many years ago by Flory and Rehner,[33] assumes uniform distributions of polymer segments and cross-linking points throughout the polymer network. NMR investigations, however, suggest the heterogeneous nature of PNIPAM particles.[34] To take into account the heterogeneity, we use an empirical modification of the Flory−Rehner theory proposed by Hino and Prausnitz.[28] This theory has been applied successfully to describe the volume transition of bulk PNIPAM gels. Because the physics for the volume transition is independent of the particle size as long as the surface effect is unimportant, the same thermodynamic model for bulk polymer gels is also applicable to microgel particles.

At swelling equilibrium, the chemical potential of water is equal inside and outside the microgel particle[46]

$$\mu_{water}^{gel} = \mu_{water}^{pure} \qquad (5)$$

The chemical potential inside the gel includes two contributions: one is the same as that in the aqueous solution of PNIPAM polymer, and the other arises from the cross-linking of polymer chains or from the gel elasticity

$$\mu_{water}^{gel} = \mu_{water}^{polymer\ solution} + \mu_{water}^{elasticity} \qquad (6)$$

The chemical potential of water in an aqueous PNIPAM

solution can be calculated from the Flory−Huggins theory

$$(\mu_{\text{water}}^{\text{polymer solution}} - \mu_{\text{water}}^{\text{pure}})/(kT) = \ln(1-\phi) + \phi + \chi\phi^2 \quad (7)$$

where ϕ is the volume fraction of PNIPAM polymer, and the Flory polymer−solvent energy parameter χ is given empirically as a function of temperature and composition[28]

$$\chi = \frac{3}{1-0.65\phi}\left[2\ln\left(\frac{5001}{1+5000\exp(2458.867/T)}\right) - \frac{4566.468}{T}\right] \quad (8)$$

Equation 8 is obtained by fitting the Flory−Huggins theory with the phase-equilibrium data for non-cross-linked PNIPAM polymer in water.[28] For microgels, the volume fraction ϕ in eq 7 corresponds to that inside of individual particles.

The second term on the right-hand of eq 6 arises from gel elasticity. This term takes into account the effect of the network formation on the chemical potential of the solvent. According to the modified Flory−Rehner theory by Hino and Prausnitz,[28] the chemical potential of water due to gel elasticity is given by

$$\mu_{\text{water}}^{\text{elasticity}}/(kT) = \frac{\phi_0}{m}\left[\left(\frac{\phi}{\phi_0}\right)^{1/3} - \left(\frac{\phi}{\phi_0}\right)^{5/3} + \left(\frac{\phi}{2\phi_0}\right)\right] \quad (9)$$

where m is the average number of segments between two neighboring cross-linking points in the gel network, and ϕ_0 is the polymer volume fraction in the reference state where the conformation of the network chains is closest to that of unperturbed Gaussian chains. Approximately, ϕ_0 is equal to the volume fraction of polymer within the microgel particles at the condition of preparation.

Substitution of eqs 6−9 into eq 5 yields

$$\ln(1-\phi) + \phi + \chi\phi^2 + \frac{\phi_0}{m}\left[\left(\frac{\phi}{\phi_0}\right)^{1/3} - \left(\frac{\phi}{\phi_0}\right)^{5/3} + \left(\frac{\phi}{2\phi_0}\right)\right] = 0 \quad (10)$$

At a given temperature, eq 10 can be used to find the polymer volume fraction ϕ. Once we have ϕ, the diameter of PNIPAM particles can be found from

$$\frac{\sigma}{\sigma_0} = \left(\frac{\phi_0}{\phi}\right)^{1/3} \quad (11)$$

where σ_0 is the particle diameter at the reference state. In this work, the average chain length m and the volume fraction of polymer ϕ_0 at the reference state are obtained by fitting eqs 10 and 11 to the diameters of microgel particles obtained from static and dynamic light scattering experiments.

3.2. Interparticle Potential and Osmotic Second Virial Coefficient. The interparticle potential $u(r)$ is related to the osmotic second virial coefficient B_2 by

$$B_2 = 2\pi\int_0^\infty [1 - e^{-u(r)/kT}]r^2\,dr \quad (12)$$

where r stands for the center-to-center distance between colloidal particles.

For the PNIPAM particles considered in this work, we assume that the interaction potential can be represented by a Sutherland-like function that includes a hard-sphere repulsion and a van der Waals attraction. A similar potential was used by Senff and Richttering for representing the phase behavior of rheological properties of PNIPAM microgel dispersions.[14] The hard-sphere diameter is related to the swelling of gel particles and can be calculated from eq 11. The van der Waals attraction beyond the hard-sphere diameter can be represented by

$$u_A(r) = -\frac{H}{r^n} \quad (13)$$

where H is the Hamaker constant. We assume $n = 8$ in considering that the range of attraction between colloidal particles (relative to the particle size) is shorter than that between atomic molecules. The calculated results is not sensitive to a small change in n when the Hamaker constant is obtained by fitting to the osmotic second virial coefficients obtained from static light scattering experiments.

Approximately, the Hamaker constant of microgel particles is given by[35]

$$H \propto {\rho_m}^2 \quad (14)$$

where ρ_m represents the number density of polymeric groups within each particle. The proportionality constant in eq 14 is independent of temperature and the polymeric group density ρ_m. Following eqs 13 and 14, we obtain the attractive potential due to the van der Waals forces

$$\frac{u_A(r)}{kT} = -k_A\left(\frac{T_0}{T}\right)\left(\frac{\sigma_0}{\sigma}\right)^{6+n}\left(\frac{\sigma}{r}\right)^n \quad (15)$$

where k_A is a dimensionless constant and T_0 is a reference temperature that is introduced for the purpose of dimensionality. In eq 15, the parameters T_0, σ_0, and k_A are temperature-independent, and they can be obtained by fitting eq 12 to the osmotic second virial coefficients obtained from static light scattering measurements.

3.3. Thermodynamic Model for the Fluid Phase. To calculate the phase diagram of microgel dispersions, we need thermodynamic models for both fluid and solid phases. For a dispersion of microgel particles in the fluid state, a first-order perturbation theory is appropriate because higher order terms are insignificant when the perturbation arises only from short-range attractions.[36] The Helmholtz energy of the fluid phase includes a hard-sphere contribution that is given by the Carnahan−Starling equation of state and a perturbation that takes into account the van der Waals attraction (eq 15). In dimensionless units, the Helmholtz energy is given by

$$\frac{F}{NkT} = \ln(\eta) - 1 + \frac{4\eta - 3\eta^2}{(1-\eta)^2} + 12\eta\int_1^\infty x^2 g_F^{HS}(x)\frac{u_A(x)}{kT}\,dx \quad (16)$$

where N represents the total number of particles, $\eta = \pi\rho\sigma^3/6$ is the particle packing fraction, ρ is the particle number density, and $g_F^{HS}(r)$ is the hard-sphere radial

distribution function. For convenience, we correlate the integral in eq 16 as a function of particle packing fraction using the radial distribution function $g_F^{HS}(r)$ obtained from the Percus−Yevick equation[37,47]

$$I_F(\eta) \equiv \int_1^\infty x^{-6} g^{HS}(x)\, dx = 0.027224\eta^2 + 0.1642\eta + 0.2007 \quad (17)$$

The quadric form as given in eq 17 is applicable to the reduced density $\rho\sigma^3 < 0.6$.

Replacement of the integral in eq 16 with $I_F(\eta)$ gives

$$\frac{F}{NkT} = \ln(\eta) - 1 + \frac{4\eta - 3\eta^2}{(1-\eta)^2} - 12\eta I_F(\eta)\epsilon^* \quad (18)$$

where

$$\epsilon^* = \frac{\epsilon}{kT} = k_A\left(\frac{T_0}{T}\right)\left(\frac{\sigma_0}{\sigma}\right)^{6+n} \quad (19)$$

Other thermodynamic properties can be derived from eq 18 following standard thermodynamic relations.

3.4. An Extended Cell Model for the Solid Phase. To describe the thermodynamic properties of the solid phase, we follow a perturbation approach similar to that for the fluid phase. The Helmholtz energy includes a contribution from the reference hard-sphere crystal and a perturbation taking into account the van der Waals attraction

$$\frac{F}{NkT} = \frac{F^{HS}}{NkT} + 12\eta\int_1^\infty x^2 g_S^{HS}(x)\frac{u_A(x)}{kT}\, dx \quad (20)$$

where $g_S^{HS}(r)$ is the radial distribution function of the hard-sphere solid. As in a hard-sphere system, an aqueous dispersion of PNIPAM microgel particles forms a face-centered-cubic (fcc) lattice in the solid phase even when the particles are at low cross-linking density ("softer" particles).[13]

According to an improved cell theory,[38] the Helmholtz energy of the hard-sphere solid is given by

$$\frac{F^{HS}}{NkT} = -\ln\left[\frac{8}{\sqrt{2}}((\rho/\rho_0)^{1/3} - 1)\right] \quad (21)$$

Compared with the original cell model proposed many years ago by Lennard-Jones and Devonshire,[39] the improved cell model introduces a factor of 8, taking into account the fact that the neighboring particles share partially the free space. Unlike the original cell model, the modified cell model provides accurate freezing and melting densities for the fluid−solid transition of uniform hard spheres. As outlined in the Appendix, the hard-sphere radial distribution function $g_S^{HS}(r)$ can be calculated using a modified Gaussian model for density distributions.

Using the radial distribution function $g_S^{HS}(r)$ for the hard-sphere solid, we numerically integrate the perturbation term in eq 20. The final expression for the Helmholtz energy of the solid phase is given by

$$\frac{F}{NkT} = -\ln\left[\frac{8}{\sqrt{2}}((\rho/\rho_0)^{1/3} - 1)\right] - 12\eta I_S(\rho)\epsilon^* \quad (22)$$

where

$$I_S(\rho) \equiv \int_1^\infty x^{-6} g_S^{HS}(x)\, dx = 0.451\rho^2 - 0.5253\rho + 0.5514 \quad (23)$$

Equation 23 is applicable for the solid phase with the reduced density $0.95 < \rho\sigma^3 < 1.27$.

3.5. Phase-Equilibrium Calculations. Once we have an expression for the Helmholtz energy, the chemical potential μ and the osmotic pressure P can be derived following standard thermodynamic relations

$$\mu = \left(\frac{\partial F}{\partial N}\right)_{T,V} \quad (24)$$

$$P = -\left(\frac{\partial F}{\partial N}\right)_{T,N} \quad (25)$$

where V stands for total volume. A fluid−fluid coexistence curve is obtained from the criteria of phase equilibrium

$$\mu^\alpha = \mu^\beta \quad (26)$$

$$P^\alpha = P^\beta \quad (27)$$

where α and β designate two distinguishable fluid phases. To calculate the pressure and the chemical potential in the fluid phase, the Helmholtz energy is given by eq 18. For each temperature, we solve for equilibrium densities ρ^α and ρ^β using eqs 26 and 27. If no solution is found, the temperature is above the critical temperature for fluid−fluid equilibrium; in this case, there is only one fluid phase.

For fluid−solid equilibrium, we also use eqs 26 and 27. But now, for phase α we use eq 18 for the liquid-phase Helmholtz energy while for phase β we use eq 22 for the solid-phase Helmholtz energy. Again, we search for densities ρ^α and ρ^β that satisfy both equations of phase equilibrium, i.e., eqs 26 and 27.

4. Results and Discussion

Static light scattering was carried out for PNIPAM microgel dilute dispersions with the concentrations from 2.5×10^{-6} to 5×10^{-6} to 1×10^{-5}. Parts a, b, and c of Figure 1 show the Zimm plots at 25, 31, and 34 °C, respectively. From the extrapolation of $KC/R_{vv}(q)$ in eq 1 to the zero angle and zero concentration, we obtained the second virial coefficient B_2 and the radius of gyration $\langle R_g \rangle$.

Table 1 and Figure 2a present the sizes of PNIPAM microgel particles from SLS and DLS measurements. The inserted plot in Figure 2a shows the ratio of the radius of gyration and the hydrodynamic radius. For a homogeneous sphere $R_g/R_h = \sqrt{3/5}$, but due to the inhomogeneity of microgel particles, R_g/R_h shown here is slightly higher. As observed by Hu and Wu for PNIPAM microgels with core−shell structures,[40] the minimum of R_g/R_h near the volume transition temperature reflects the nonuniform volume change within individual particles. It appears that near the volume transition point the PNIPAM chains inside the particle collapse while the dangling chains outside make the hydrodynamic radius less sensitive. As a result, the ratio of the two radii shows a minimum. Both the radius of gyration and the hydrodynamic radius indicate that the microgel particles undergo a continuous volume transition around 34 °C, in close agreement to that for neutral bulk PNIPAM gels. If the microgels were

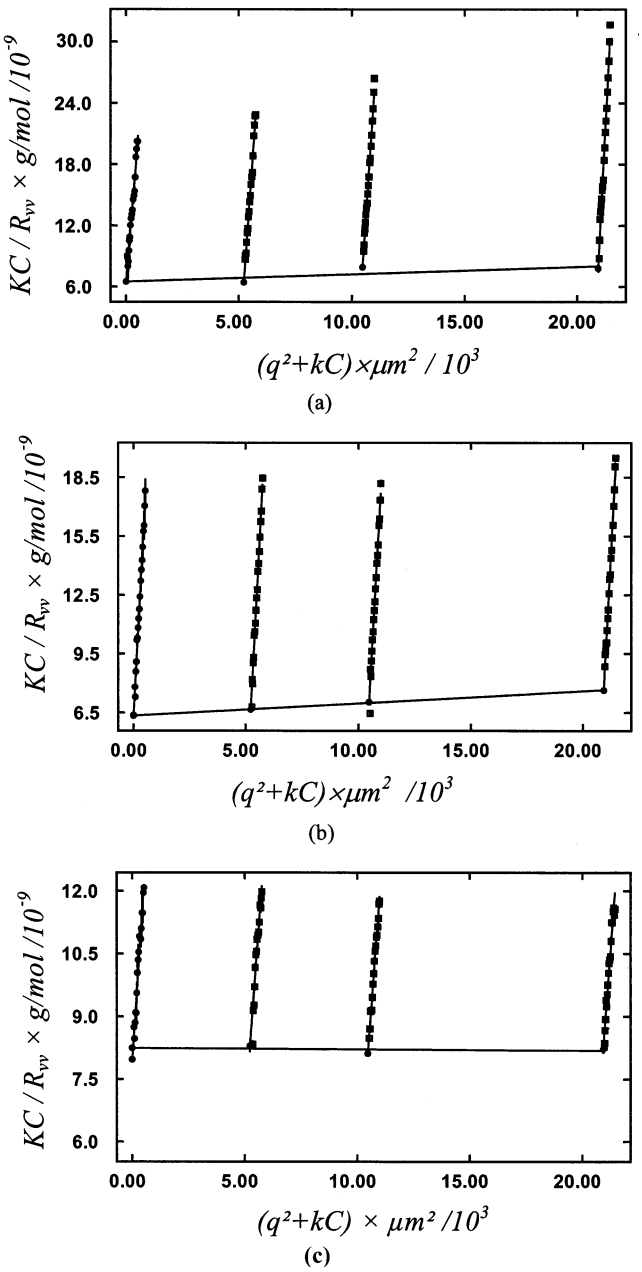

Figure 1. Zimm plots of the PNIPAM microgel particles dispersed in water at three temperatures: (a) 25.0, (b) 31.0, and (c) 34.0 °C.

Table 1. Radius of Gyration from SLS, Hydrodynamic Radius from DLS, and the Average Radius from Eq 28

T (°C)	R_g (nm)	R_h (nm)	$(R_h + \sqrt{5/3}\,R_g)/2$ (nm)
25	112	133	139
28	104	121	128
31	93.3	111	116
33	74.9	107	102
34	51.3	79.3	72.8
35	49.9	61.3	62.9
37	45.5	54.1	56.4

significantly charged, they would show discontinuous volume transitions.[17] Figure 2b shows the distribution functions for the radius of PNIPAM microgels at temperatures below and above the volume transition. The distribution function of the hydrodynamic radius is directly related to $G(\Gamma)$ by changing the independent variable from Γ to R_h using eq 4. Below the volume transition temperature, the microgels are in their swollen state and are narrowly distributed, while above the volume transition temperature, the microgels shrink sharply but still are fully dispersed.

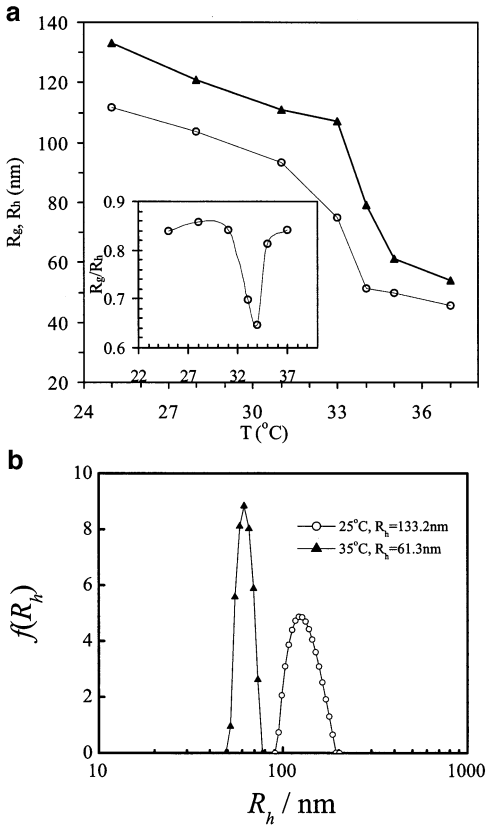

Figure 2. (a) Hydrodynamic radius and gyration radius of PNIPAM microgels in water at different temperatures. The inserted plot shows the ratio of the radius of gyration and the hydrodynamic radius. (b) Hydrodynamic radius distributions of PNIPAM microgel spheres in water at $T = 25$ and 35 °C. Here the microgel concentration is $C = 5 \times 10^{-6}$g/g, and the scattering angle is 60°.

To correlate the radius of PNIPAM gel particles as a function of temperature, we combine the radius of gyration R_g with the hydrodynamic radius R_H from respectively static and dynamic light scattering measurements. By assuming that the microgel particles are homogeneous spheres, we define the effective radius

$$R = (\sqrt{5/3}R_g + R_H)/2 \qquad (28)$$

This effective radius is introduced for representing the excluded volume of microgel particles as required in phase equilibrium calculations. Figure 3 presents the radius of microgel particles near the volume-transition temperature (approximately at 34. 3°C). The error bars give the difference between hydrodynamic radius and the radius of gyration. The solid line is calculated using the modified Flory−Rehner theory (eqs 10 and 11). In the calculation of the particle radius, the polymer fraction at the condition of preparation $\phi_0 = 0.0884$, the average number of segments between two neighboring cross-linking points $m = 34$, and the particle radius at the preparation condition $R_0 = 125.8$ nm are obtained by fitting to the experimental data. These model parameters are in good agreement with experiments. Figure 3 indicates that the volume transition of PNIPAM particles can be successfully correlated using the modified Flory−Rehner theory.

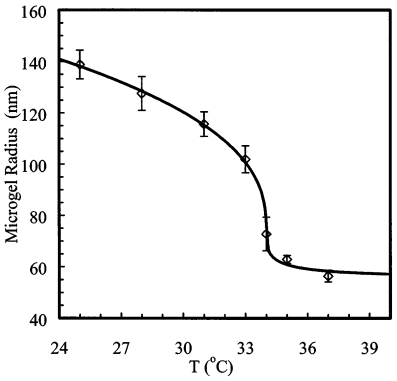

Figure 3. Radius of PNIPAM particles vs temperature. The points are averages from dynamic and static light scattering measurements with the error bars showing the differences between the two. The line is calculated from eq 10.

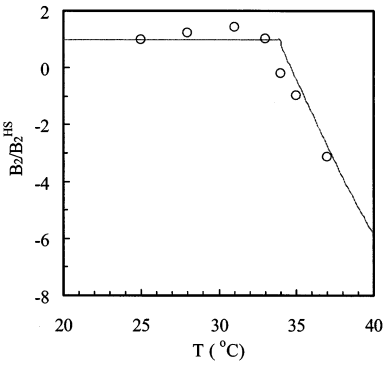

Figure 4. Reduced osmotic second virial coefficients (B_2/B_2^{HS}) for PNIPAM particles dispersed in pure water. Points are from static light scattering, and the line is calculated from eq 12 normalized by the second virial coefficient $B_2^{HS} = (2\pi/3)\sigma^3$ for the corresponding hard spheres.

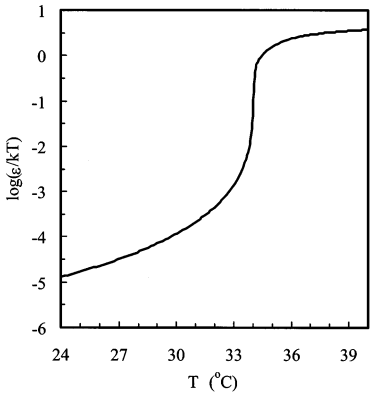

Figure 5. Reduced energy parameter (ϵ/kT) for interparticle potential between PNIPAM particles near the volume-transition temperature.

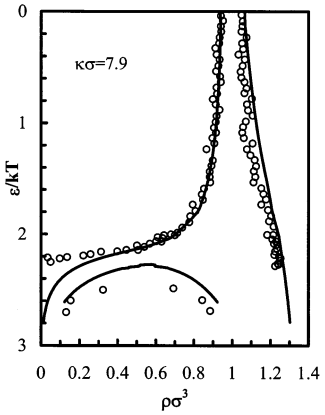

Figure 6. Phase diagram of a typical colloidal system with weak attractive forces. Points are from simulation data for Yukawa potential by Hagen and Frenkel,[41] and the lines are from the theory.

Figure 4 presents the reduced osmotic second virial coefficients (B_2/B_2^{HS}) for microgel particles dispersed in water. The hard-sphere second virial coefficient is related to the particle diameter σ by $B_2^{HS} = (2\pi/3)\sigma^3$. In Figure 4, the open circles are data points from static light scattering measurements, and the line is calculated using eqs 12 and 15, with the molecular weight $M_W = 1.73 \times 10^7$ g/mol and the proportional constant $k_A = 6.43 \times 10^{-5}$ obtained by fitting to the experimental data. A positive osmotic second virial coefficient means that the overall interparticle potential is repulsive; otherwise, it is attractive. Figure 4 shows that below the volume-transition temperature the PNIPAM particles behavior essentially like hard spheres. In this case, the microgel particles are in the swollen state, and they contain up to 97 vol % of water. The van der Waals attraction between colloidal particles is negligible due to the close match in the Hamaker constants of the particle and the water. The reduced osmotic second virial coefficient exhibits a sharp change at the volume transition temperature and beyond which it turns to negative, indicating an increase in the van der Waals attraction as the particles collapse. Figure 4 suggests that, with temperature-dependent size and energy parameters, the Sutherland-type function captures the essential features of the interaction potential between microgel particles.

Figure 5 shows the reduced energy parameter, $\epsilon/(kT)$, near the volume-transition temperature as obtained by correlation with the osmotic second virial coefficients from experimental. Experiments values for this parameter are not included because it is difficult to make a direct (or indirect) measurement of the reduced energy parameter. But the credibility of calculated results is implied in the comparison of the osmotic second virial coefficients as shown in Figure 4. Remarkably, the energy parameter increases over 6 orders of magnitude as temperature changes from 24 to 36 °C, with the sharpest increase at the volume transition temperature of 34 °C. Whereas the volume transition of polymer gels has been extensively studied, we are not aware of any published work on the drastic effect of volume transition on the interparticle potential.

To calibrate the thermodynamic models proposed in this work, we first consider the phase behavior of a Yukawa system that is often used to represent colloidal dispersions with weak attractive interactions. Figure 6 compares the fluid−solid as well as metastable fluid−fluid coexistence curves from simulation[41] and from the perturbation theory. The agreement is satisfactory except near the critical point of the fluid−fluid equilibrium where the long-range fluctuations become significant. An improved prediction in this region can be achieved by applying the renormalization group theory.[42] Figure 6 indicates that at high temperature the system is dominated by short-range repulsion, and it exhibits a freezing transition similar to that for hard spheres. While at low temperature, freezing occurs at dilute condition, and it is separated by a metastable liquid−liquid equilibrium.

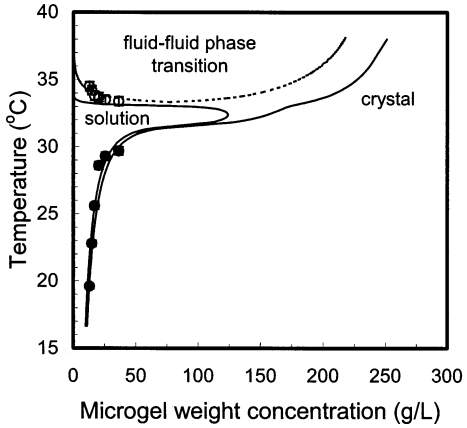

Figure 7. Phase diagram of aqueous dispersions of PNIPAM particles determined from turbidity measurements (symbols) and from the thermodynamic perturbation theory with an empirical correction of temperature (lines). The filled and open circles represent respectively the melting and the second phase-separation temperatures.

Figure 7 shows the calculated phase diagram of PNIPAM microgel dispersion using the first-order perturbation theory for the fluid phase (eq 18) and the corrected cell model for the solid phase (eq 22). Also shown in this figure are results from experimental measurements. In this calculation, the calculated temperature is rescaled empirically by $T' = T(15/R_g)^{0.005}$ to match the experimental results quantitatively. The discrepancy is probably because the effect of osmotic pressure on the particle size is neglected in the perturbation theory or because the slight size difference (~2 nm) between the microgel samples used in light scattering and in turbidity measurements. Nevertheless, the theory and experiment agree, as least semiquantitatively. The interesting phase diagram as shown in Figure 7 has not been reported before.

The phase diagram shown in Figure 7 differs drastically from that of a conventional colloidal dispersion or that of a colloid polymer mixture.[2] Below the volume-transition temperature, the coexistence phases at the freezing and melting points have close particle densities, similar to that observed in a hard-sphere system. However, above the volume-transition temperature, the fluid−solid transition spans over a wide gap of particle concentrations. At high temperature, the fluid phase at the freezing point is highly dilute while the solid phase at the melting point is highly concentrated. Interestingly, this phase diagram indicates that a microgel dispersion can freeze at temperatures both above and below the gel volume-transition temperature. For instance, according to this phase diagram, a microgel dispersion with 7 g/L particle concentration is in the fluid state at 34.5 °C; it becomes a solid of similar density when the temperature drops to about 34 °C, and the dispersion will be separated into a dilute solution and a solid of much higher density (about 17 g/L) at about 35.3 °C.

The dashed line in Figure 7 shows a metastable fluid−fluid coexistence curve with a low critical solution temperature. This coexistence curve is a reminiscence of that for an aqueous solution of un-cross-linked PNIPAM polymer. Because of strong hydrogen bonding with water molecules from CO and NH groups, PNIPAM can be dissolved in water at a low temperature. In this case, the isopropyl groups along the PNIPAM chain are caged by water molecules. When the temperature is increased, the cages of water molecules are partially melted, resulting in entropy increases. As a result, upon the increase of the temperature, the hydrophobic attraction due to the isopropyl groups and due to the polymer backbone becomes more important and the solubility of PNIPAM in water drops.

Figure 7 also shows the phase transitions in aqueous PNIPAM dispersions determined using a UV−vis spectrometer. In the crystalline phase, the UV−vis spectrum exhibits a sharp attenuation peak due to the Bragg diffraction. At the crystalline melting temperature (indicated by solid circles), the peak disappears. As the temperature rises to the phase separation temperature (indicated by open circles), the turbidity increases drastically in the entire visible frequency range, signaling a phase separation. Similar structural changes have been observed from SANS experiments.[43] The experiment confirms the phase transition "loop" in the solution side as predicted by the thermodynamic theory and indicates that PNIPAM microgel dispersion shows phase transitions at both high and low temperatures. The phase transition at low temperature is similar to that for a conventional colloid, and at high temperature, it is driven by the dramatic increase in interparticle potentials as shown in Figure 5. While at a low temperature the solid phase exhibits apparent characteristics of a colloidal crystal, the phase-separated state at high temperature is much like a glass that is probably related to the metastable fluid−fluid equilibrium. In the presence of a metastable fluid−fluid equilibrium, fast kinetics of the fluid−fluid transition leads to an amorphous fluid phase of high particle concentration.

5. Conclusions

We have investigated the volume-transition equilibrium and the interaction potential between neutral PINPAM particles dispersed in pure water using static and dynamic light scattering experiments. We show that the modified Flory−Rehner theory gives an excellent description of the microgel swelling equilibrium. Using the temperature-dependent size and energy parameters, the Sutherland-like potential provides a reasonable representation of the interparticle potential for PNIPAM particles in swollen and in collapsed phases. The phase diagram calculated from a first-order perturbation theory and an extended cell model indicates that an aqueous dispersion of PNIPAM particles can freeze at both high and low temperatures. At low temperature, the freezing occurs at large particle volume fraction, similar to that in a hard-sphere system, while at high temperature, the freezing occurs at low particle concentration, driven by the strong van der Waals attraction due to the collapsed microgel particles. The calculated phase diagram has been confirmed semiquantitatively by experiments.

In many aspects, the phase behavior of colloidal dispersions reassembles that for simple fluids. However, a noticeable difference is that, unlike the vapor−liquid equilibrium of a simple fluid, the equilibrium between a dilute and a concentrated colloidal dispersion is often metastable. Whereas that difference, arising for the short-ranged solvent-mediated attraction between colloidal particles, is now well-documented, not much attention has been given to other features that are unique in colloidal systems. The temperature-dependent potential as shown in this work is special in colloidal systems. Because the interparticle potential is strongly

temperature-dependent, the phase behavior of PNIPAM dispersions differs remarkably from that for simple fluids or for conventional colloids. In future work it might be interesting to investigate other features that are special to colloidal dispersions, including the multibody effect on the phase behavior and dissimilarity of interparticle potential in different phases.

Acknowledgment. J.W. gratefully acknowledges the financial support from the University of California Energy Research Institute. Z.H. gratefully acknowledges the financial support from the National Science Foundation under Grant DMR-0102468, the U.S. Army Research Office under Grant DAAD19-01-1-0596, and the Texas Advanced Technology Program. We thank B. Zhou for his technical assistance.

Appendix. Radial Distribution Function of a Hard-Sphere Solid

To obtain the radial distribution function of hard spheres in an fcc lattice, we use a procedure similar to that proposed by Rascon et al.[44] The radial distribution function around an arbitrary tagged particle can be represented by the summation of an empirical exponential function for the first layer and Gaussian distributions in the remaining layers:

$$g_S^{HS}(x) = \frac{A}{x} e^{-\alpha_1(x-R_1)/2} + \frac{1}{24\eta}\sqrt{\alpha/2\pi}\sum_{i\geq 2}\frac{n_i}{xR_i}[e^{-\alpha(x-R_i)/2} + e^{-\alpha(x+R_i)/2}] \quad \text{(A1)}$$

In eq A1, $x = r/\sigma$, n_i is the number of particles in the ith neighboring layer from the tagged particle, R_i represents the center-to-center distance between a particle in the ith layer and the tagged particle, and A, α_1, and α are yet-to-be determined parameters. For an fcc lattice, the Gaussian parameter α in eq A1 is related to particle density

$$\alpha = \left(\frac{\sqrt{3}\pi}{4}\right)^{2/3}\left[\left(\frac{\sqrt{2}}{\rho\sigma^3}\right)^{1/3} - 1\right]^{-2} \quad \text{(A2)}$$

The parameters A, α_1, and R_1 in eq A1 can be determined by requiring that the radial distribution function gives the exact number of particles within the first layer, the exact mean distance between immediate neighboring particles, and a contact value that is consistent with the corresponding equation of state. By imposing these requirements, the parameters A, α_1, and R_1 can be solved from

$$4\pi\rho A\int_1^\infty x e^{-\alpha_1(x-R_1)/2}\,dx = n_1 \quad \text{(A3)}$$

$$\frac{4\pi\rho}{n_1}\int_1^\infty x^2 e^{-\alpha_1(x-R_1)/2}\,dx = R_1 \quad \text{(A4)}$$

$$z = 1 + 4\eta A e^{-\alpha_1(1-R_1)/2} \quad \text{(A5)}$$

where z stands for the compressibility factor of the hard-sphere solid. According to the modified cell model, the compressibility factor z is given by

$$z = 1/[1 - (\rho\sigma^3/\sqrt{2})^{1/3}] \quad \text{(A6)}$$

In this work, we assume that the correlation beyond the first five lattice layers does not make significant contribution to the thermodynamic properties. The numbers of particles (n_i) in the first fives layers are given by[45]

$$(12, 6, 24, 12, 24) \quad \text{(A7)}$$

and the corresponding distances (R_i) from the central particle, in units of lattice constant a, are

$$(1, \sqrt{2}, \sqrt{3}, \sqrt{4}, \sqrt{5}) \quad \text{(A8)}$$

References and Notes

(1) Pusey, P. N. In *Liquid, Freezing, and the Glass Transition*; Les Houches, J. P., Levesque, H. D., Zinn-Justin, J., Eds.; Elsevier: Amsterdam, 1990.
(2) Poon, W.; Pusey, P.; Lekkerkerker, H. *Phys. World* **1996**, *9*, 27−32.
(3) Frenkel, D. *Science* **2002**, *296*, 65−66.
(4) Velev, O. D.; Lenhoff, A. M.; Kaler, E. W. *Science* **2000**, *287*, 2240−2243.
(5) Xia, Y. N.; Gates, B.; Yin, Y.; Lu, Y. *Adv. Mater.* **2000**, *12*, 693−713.
(6) Pelton, R. H.; Chibante, P. *Colloids Surf.* **1986**, *20*, 247−256.
(7) Pelton, R. *Adv. Colloid Interface Sci.* **2000**, *85*, 1−33.
(8) Saunders, B. R.; Vincent, B. *Adv. Colloid Interface Sci.* **1999**, *80*, 1−25.
(9) Kawaguchi, H. *Prog. Polym. Sci.* **2000**, *25*, 1171−1210.
(10) Fernandez-Nieves, A.; Fernandez-Barbero, A.; Vincent, B.; de las Nieves, F. J. *Macromolecules* **2000**, *33*, 2114−2118.
(11) Laukkanen, A.; Hietala, S.; Maunu, S. L.; Tenhu, H. *Macromolecules* **2000**, *33*, 8703−8708.
(12) Gao, J.; Hu, Z. B. *Langmuir* **2002**, *18*, 1360−1367.
(13) Hellweg, T.; Dewhurst, C. D.; Bruckner, E.; Kratz, K.; Eimer, W. *Colloid Polym. Sci.* **2000**, *278*, 972−978.
(14) Senff, H.; Richtering, W. *J. Chem. Phys.* **1999**, *111*, 1705−1711.
(15) Hu, Z. B.; Wang, C. J.; Chen, Y. Y.; Zhang, X. M.; Li, Y. *J. Polym. Sci., Part B: Polym. Phys.* **2001**, *39*, 2168−2174.
(16) Debord, J. D.; Lyon, L. A. *J. Phys. Chem. B* **2000**, *104*, 6327−6331.
(17) Hirotsu, S.; Hirokawa, Y.; Tanaka, T. *J. Chem. Phys.* **1987**, *87*, 1392.
(18) Peppas, N. A.; Huang, Y.; Torres-Lugo, M.; Ward, J. H.; Zhang, J. *Annu. Rev. Biomed. Eng.* **2000**, *2*, 9−29.
(19) Martinez-Rubio, M. I.; Ireland, T. G.; Fern, G. R.; Silver, J.; Snowden, M. J. *Langmuir* **2001**, *17*, 7145−7149.
(20) Weissman, J. M.; Sunkara, H. B.; Tse, A. S.; Asher, S. A. *Science* **1996**, *274*, 959−960.
(21) Lee, K.; Asher, S. A. *J. Am. Chem. Soc.* **2000**, *122*, 9534−9537.
(22) Hu, Z. B.; Lu, X. H.; Gao, J. *Adv. Mater.* **2001**, *13*, 1708−1712.
(23) Wu, J. Z.; Sassi, A. P.; Blanch, H. W.; Prausnitz, J. M. *Polymer* **1996**, *37*, 4803−4808.
(24) Ogawa, K.; Wang, B.; Kokufuta, E. *Langmuir* **2001**, *17*, 4704−4707.
(25) Gilanyi, T.; Varga, I.; Meszaros, R.; Filipcsei, G.; Zrinyi, M. *Phys. Chem. Chem. Phys.* **2000**, *2*, 1973−1977.
(26) Saunders, B. R.; Crowther, H. M.; Morris, G. E.; Mears, S. J.; Cosgrove, T.; Vincent, B. *Colloid Surf. A* **1999**, *149*, 57−64.
(27) Wu, C.; Zhou, S. Q.; Auyeung, S. C. F.; Jiang, S. H. *Angew. Makromol. Chem.* **1996**, *240*, 123−136.
(28) Hino, T.; Prausnitz, J. M. *J. Appl. Polym. Sci.* **1996**, *62*, 1635−1640.
(29) Zimm, B. H. *J. Chem. Phys.* **1948**, *16*, 1099.
(30) Gao, J.; Hu, T. J.; Zhang, Y. B.; Li, P.; Wu, C. *Chin. J. Polym. Sci.* **1999**, *17*, 595.
(31) Schmitz, K. S. *An Introduction to Dynamic Light Scattering by Macromolecules*; Academic Press: Boston, MA, 1990.
(32) Provencher, S. W. *Makromol. Chem.* **1979**, *180*, 201.
(33) Flory, P. J. *Principles of Polymer Chemistry*; Cornell University Press: Ithaca, NY, 1953.
(34) Guillermo, A.; Addad, J. P. C.; Bazile, J. P.; Duracher, D.; Elaissari, A.; Pichot, C. *J. Polym. Sci., Part B: Polym. Phys.* **2000**, *38*, 889−898.

(35) Israelachvili, J. N. *Intermolecular and Surface Forces*, 2nd ed.; Academic Press: London, 1992.
(36) GilVillegas, A.; Galindo, A.; Whitehead, P. J.; Mills, S. J.; Jackson, G.; Burgess, A. N. *J. Chem. Phys.* **1997**, *106*, 4168−4186.
(37) Hansen, J. P.; McDonald, I. R. *Theory of Simple Liquids*, 2nd ed.; Academic Press: London, 1986.
(38) Wu, J. Z.; Prausnitz, J. *Fluid Phase Equilib.* **2002**, *194*, 689−700.
(39) Lennard-Jones, J. E.; Devonshire, A. F. *Proc. R. Soc. London, Ser A* **1937**, *163*, 53.
(40) Hu, T. J.; Wu, C. *Phys. Rev. Lett.* **1999**, *83*, 4105−4107.
(41) Hagen, M. H. J.; Frenkel, D. *J. Chem. Phys.* **1994**, *101*, 4093−4097.
(42) Lue, L.; Prausnitz, J. M. *J. Chem. Phys.* **1998**, *108*, 5529−5536.
(43) Kratz, K.; Hellweg, T.; Eimer, W. *Polymer* **2001**, *42*, 6631−6639.
(44) Rascon, C.; Mederos, L.; Navascues, G. *Phys. Rev. E* **1996**, *54*, 1261−1264.
(45) Hirschfelder, J. D.; Curtis, C. F.; Bird, R. B. *Molecular Theory of Gases and Liquids*; Wiley: New York, 1964.
(46) Because the osmotic pressure of microgel dispersion is small in comparison to the gel swelling pressure, the microgel particle concentration has only negligible effect on the chemical potential of water.
(47) Alternative correlations for eq 17 are possible, but the calculated thermodynamic properties are insensitive the specific form of $I_F(\eta)$.

MA025656M